Biochemical and Biophysical Research Communications 745 (2025) 151217

Contents lists available at ScienceDirect

Biochemical and Biophysical Research Communications

journal homepage: www.elsevier.com/locate/ybbrc

The mechanism of autoreduction in Dehaloperoxidase-A

Jing Zhao, Yinglu Chen, Hunter Alford, Stefan Franzen *

Department of Chemistry, North Carolina State University, Raleigh, NC, 27695, USA

A B S T R A C T

Hemoglobin and myoglobin are known to undergo autoxidation, in which the oxyferrous form of the heme is oxidized to the ferric state by O_2. Dehaloperoxidase-A (DHP-A), a multifunctional catalytic hemoglobin from *Amphitrite ornata* is an exception and is observed to undergo the reverse process, during which the ferric heme is spontaneously reduced to the oxyferrous form under aerobic conditions. The high reduction potential of DHP (+202 mV at pH 7.0) partially explains this unusual behavior, but the endogenous source of reducing equivalents has remained obscure. Cysteine, methionine, tyrosine, and tryptophan are the principal endogenous reducing agents in proteins that may explain the observed autoreduction in DHP-A. In fact, DHP-A has six methionines, which may be of particular importance for the observed autoreduction. To investigate the role of the sulfur-containing residues, we created seven mutants (C73S, C73 S/M49C, S78C, M63L, M64L, M63 L/M64L, and H55V) by site-directed mutagenesis and conducted a series of CO-driven autoreduction kinetic measurements. Mutational analysis suggests a role for the pair of methionines M63 and M64 increaing the autoreduction rate. Adding surface cysteines has little effect, but the C73S mutation that eliminates the only native surface cysteine accelerates the autoreduction process. The kinetics had a sigmoidal form which was found to be a result of anti-cooperative behavior. This observation suggests that DHP-A's monomer-dimer equilibrium in solution may play a role in regulating the autoreduction process.

1. Introduction

The primary function of hemoglobins and myoglobins is oxygen storage and transport. This function requires the heme to be in the ferrous state. However, hemoglobins and myoglobins are susceptible to oxidation and denaturation following a well-studied autoxidation mechanism [1–3]. In fact, autoxidation has been considered a common property of heme proteins [4]. This naturally occurring process in the presence of diatomic oxygen is sufficiently rapid that most oxyferrous hemoglobins and myoglobins will be oxidized to the ferric state a few hours or less under aerobic conditions in solution [1]. Autoxidation becomes especially rapid for acellular hemoglobin in the absence of an intrinsic reducing system [5]. However, heme proteins with high reduction potentials and a sufficient number reducing amino acids will spontaneously to react to form the ferrous state in a process known as autoreduction.

The autoxidation of hemoglobin and myoglobin not only generates reactive oxygen species (ROS) such as superoxide radical and hydrogen peroxide but can also degrade the protein to release free heme in the cellular environment [6–8]. To suppress oxidative stress, a number of antioxidant proteins such as peroxiredoxin, thioredoxin, sulfiredoxin and methionine sulfoxide reductase will catalytically react with reactive oxygen species (ROS) by utilizing redox-active Cys or Met amino acids [9–11]. Sulfur-containing residues like Cys and Met can also function as internal reducing reagents. In some proteins oxidized Cys and Met are enzymatically regenerated by NADPH reductases [12–15].

Herein, we report that DHP-A cloned from *Amphitrite* undergoes an autoreduction process, during which ferric heme is gradually reduced to the ferrous state without involvement of an external reductant. This unique biochemical behavior contrasts with the autoxidation process that is well-known among the great majority of hemoglobins and myoglobins. The reduction potentials of most globins fall in the range from +50 mV to +150 mV at the high end. DHP-A has an exceptionally high redox potential which provides a plausible pathway for DHP-A to switch between its functions as a catalytic enzyme and an oxygen carrier owing to reduction of heme by endogenous amino acids. DHP-A and -B are two multifunctional proteins [16,17] whose high reduction potentials (+202 mV and +193 at pH 7.0) may relate to functional switching by changing the oxidation state of the heme [18,19]. When referring to both isozymes the designation DHP can be used. When compared to mammalian myoglobin and hemoglobin α, β subunits the sequence homology with DHP is less than 20 % [20,21]. Both isozymes of DHP have only one cysteine residue in its peptide sequence, Cys73, which is analogous to Cys110 in human myoglobin [22,23]. Cys73 is located on the surface of the protein in the dimer interface observed in the X-ray crystal structure of every form of DHP studied [24–26]. Both DHP isozymes have six methionine residues at sites distributed over both helical and loop regions. NMR relaxation experiments on DHP showed that 5 out 7 of the sulfur-containing residues (Met49, Met69, Met108, Met136 and Cys73) in DHP-A experience significant chemical exchange on their

* Corresponding author.
E-mail address: franzen@ncsu.edu (S. Franzen).

https://doi.org/10.1016/j.bbrc.2024.151217
Received 15 October 2024; Received in revised form 18 December 2024; Accepted 18 December 2024
Available online 19 December 2024

backbone amide N–H groups [27]. Chemical exchange on these residues is relevant to conformational change or interaction with other molecules on the microsecond to millisecond time scale [28]. In this study we investigate the role of a Met and Cys pool of amino acids that appears to maintain DHP in the ferrous state, but also may be related to radical transfers that ultimately lead to protein-heme crosslinking [29].

The reactivity of the Met/Cys pool parallels the group of five tyrosines in DHP-A (Tyr16, Tyr28, Tyr34, Tyr38, Tyr107). Freeze quench EPR studies have shown that DHP-A has Tyr pool that provides a charge transfer network related to its peroxidase function [30,31]. The evidence presented here can be combined with observations of DHP deactivation via heme-protein crosslinking to show that Cys and Met regulate internal electron transfer (ET) to protect DHP from oxidative damage while the Tyr amino acids are important for rapid proton-coupled electron transfer (PCET) in peroxidase activity [29]. Given the antioxidant properties of the sulfur-containing amino acid residues [15], it is plausible to postulate that cysteine and methionine are the major source of reducing power inside the protein because both residues are subject to reversible redox reactions by forming a disulfide bond or methionine sulfoxide, respectively. The standard redox potential for the two electron oxidation of methionine to methionine sulfoxide is +160 mV [32] and that for cysteine is +220 mV [33]. While Tyr and Cys are both clear examples of closely coupled PCET, Met has less obvious coupling to proton transfer. A single Met oxidation can lead to a heme-protein crosslink. A two-electron transfer leads to sulfoxide formation, which involves binding to the oxygen atom of water and releasing two H^+, hence a coupling to deprotonation.

A single cysteine introduced in sperm whale myoglobin (SWMb) by site-directed mutagenesis will accelerate reduction in the presence of CO, while simultaneously forming disulfide bonds [14,34]. In this mechanism, formation of a disulfide bond liberates two electrons for transfer to reduce the heme. In principle, similar autoreduction of the heme Fe by Met is possible. While there are six Met amino acids in DHP-A, SWMb has two Met residues which are not known to be electroactive. In addition to the effect of concentration, pH, and substrate binding, seven Cys/Met mutants have been made to study the role of sulfur-containing amino acids in DHP-A autoreduction. Contrary to the observations in SWMb [34], the interaction of DHP dimers appears to be anti-cooperative. Fig. 1 depicts a role for the monomer-dimer equilibrium in solution which was observed previously in small-angle X-ray scattering (SAXS) studies of DHP-A [35]. Dimerization in DHP-A can be non-covalent, but can also potentially involve disulfide bond formation. In fact, autoreduction of DHP could be a pathway for functional switching between peroxidase or peroxygenase active forms that primarily use the ferric state as a catalytic resting state and the ferrous stated required for oxygen storage or gas sensor functions [17,36,37].

2. Material and methods

2.1. Materials

All Chemicals were purchase from Sigma-Aldrich and Fisher Scientific and used without further purification. A compressed CO gas tank was procured from Machine and Welding Supply Company containing 10 % CO in Argon at 1 atm. The E. Z.N.A plasmid DNA mini kit was from Omega bio-tek. The QuickChange II site-directed mutagenesis kit was purchased from Agilent Technologies Inc. The designed oligonucleotide primers were synthesized by IDT DNA Technology Inc. Horse heart myoglobin (HHMb) was obtained from Sigma-Aldrich.

2.2. Site-directed mutagenesis and protein purification

Six mutations were generated with the Quickchange II site-directed mutagenesis kit. Mutagenesis [melt (95 °C, 60 s), anneal (55 °C, 30 s), and extension (68 °C, 6min)] was performed for 18 cycles. The plasmid encoding wild type (WT) DHP-A (6XHis-tag) was used as a template to generate mutated plasmid using the designed primers (Table 1). The M63L&M64L double mutant was made by Genewiz Inc. The mutated plasmids were extracted using an E. Z.N.A plasmid DNA mini kit after the transformation of the reaction mixture into the BL21 (DE3) *E. coli*. The plasmids were then sent for sequencing at Genewiz Inc to confirm that the desired mutation was made. WT DHP-A and all mutants were expressed and purified as previously described [38]. Special care was taken for S78C mutant because the protein starts to aggregate after the oxidation by potassium ferricyanide K_3 [$Fe(CN)_6$] during the purification. Except for H55V mutant, which has a ferric state Soret band at 394 nm with $\varepsilon_{394nm} = 121{,}300\ M^{-1}cm^{-1}$, all other mutants and WT DHP-A have Soret bands at 406 nm with extinction coefficient $\varepsilon_{407nm} = 116{,}400\ M^{-1}cm^{-1}$. HHMb has a Soret band at 409 nm with extinction coefficient $\varepsilon_{409nm} = 188{,}000\ M^{-1}cm^{-1}$.

Plasmid encoded recombinant sperm whale myoglobin (SWMb) was obtained from Addgene and transformed in the BL21 (DE3) *E. coli*. The recombinant SWMb was purified according to the reported protocol

Table 1
DNA sequences of primers.

Primer	Sequence
C73S forward	5′- GAC CGA GCC ACC GAT TCT GTC CCC CTT GCG TCC -3′
C73S reverse	5′- GGA CGC AAG GGG GAC AGA ATC GGT GGC TCG GTC -3′
M49C forward	5′- CAA GAG CTC AAG TCA TGC GCC AAG TTC GGT GAT -3′
M49C reverse	5′- ATC ACC GAA CTT GGC GCA TGA CTT GAG CTC TTG -3′
S78C forward	5′- GTC CCC CTT GCG TGC GAC GCC AAC ACA CTC -3′
S78C reverse	5′- GAG TGT GTT GGC GTC GCA CGC AAG GGG GAC -3′
M63L forward	5′- AAA GTG TTC AAC CTG CTG ATG GAA GTT GCG GAC -3′
M63L reverse	5′- GTC CGC AAC TTC CAT CAG CAG GTT GAA CAC TTT -3′
M64L forward	5′- GTG TTC AAC CTG ATG CTG GAA GTT GCG GAC CGA -3′
M64L reverse	5′- TCG GTC CGC AAC TTC CAG CAT CAG GTT GAA CAC -3′

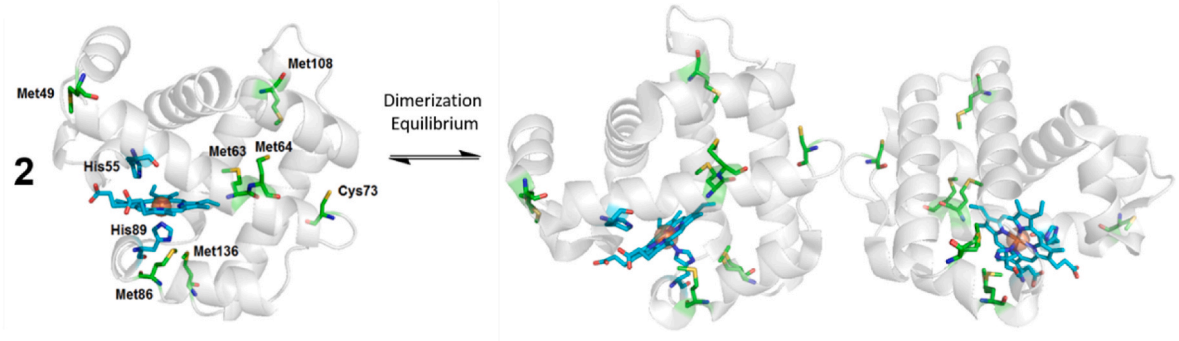

Fig. 1. DHP-A monomer – dimer equilibrium with sulfur containing residues labeled on the secondary structure.

using an ammonium sulfate precipitation method as the first step [39]. Then SWMb was completed oxidized by potassium ferricyanide followed by elution through a NAP-25 size exclusion column (GE Healthcare) to remove ferricyanide and ferricyanide. The oxidized ferric SWMb was further purified by running through the CM Sepharose Fast Flow cation exchange column (GE Healthcare). The UV–Vis spectra of purified SWMb was identical to that in the literature. The protein concentration was determined by monitoring the Soret band at 409 nm with extinction coefficient $\varepsilon_{409nm} = 171{,}000\ M^{-1}cm^{-1}$.

2.3. Autoreduction kinetics measurement

An aliquot of ~1 mL protein in 100 mM potassium phosphate (KP_i) buffer at pH 7.0 was added with 200 μL 5 mM tris(2-carboxyethyl) phosphine (TCEP) solution followed by incubation for 1 h to reduce the possible disulfide crosslinks in DHP. As a consequence of the high redox potential of ferric DHP-A (+221 mV) [18,19], the ferric protein was also reduced to the oxyferrous state by TCEP under aerobic conditions. This is noteworthy since TCEP does not reduce most other heme proteins. To remove remaining TCEP in the solution, the protein aliquot was first run through the NAP-25 column, and then the protein fraction was completely oxidized to ferric state by potassium ferricyanide and eluted through a NAP-25 column again to remove excess ferricyanide and ferrocynaide ion. A 1200 μL 50 μM protein solution aliquot was made and transferred to a conical vial sealed by septum cap. The protein solution was saturated with 10 % CO gas under 1 atm at room temperature. The Henry's law constant for CO at 298 K is $9.71 \bullet 10^{-4}$ M atm^{-1}. Therefore, the CO concentration is estimated to be circa 100 μM in the solution, which is in excess compared to the protein concentration. Because CO diffusion and binding to the protein ($k_{on} \sim 10^5$–$10^6\ M^{-1}\ s^{-1}$) is much faster than the overall reduction rate [37], the rate limiting step for autoreduction is the PCET process that reduces the ferric heme to the ferrous state.

The inhibitor 4-bromophenol (4-BP) and substrate 2,4-dibromophenol (2,4-DBP) were added in some of the experiments to test the effect of tight binding or sterically well-defiled substrates [40]. Both molecules are known to bind internally in the distal pocket of DHP, thus precluding the binding of CO. The protein solution was exchanged and filled with N_2 gas for 5 min, then exchanged and filled with 10 % CO/90 % N_2 gas for another 5 min. The solution was left to equilibrate with CO gas for another 30 min before transferring ~600 μL into a 1 mm pathlength quartz cuvette sealed with septum cap. The cuvette was fixed by a special holder and then placed in the Agilent 8453 diode array UV–visible spectrophotometer equipped with a Peltier-cooled sample cell that set a constant temperature at 37 °C. The UV–Vis spectrometer is then set to run for 10–60 h with a scan every 10 min.

2.4. Autoreduction kinetic model

The proposed autoreduction mechanism involves competing monomer and dimer pathways. The monomer ET rate is faster because Cys73 is available to act as a reductant, but also because there are fewer constraints on the dynamics of the methionines in DHP-A; Met136, Met108, Met86, Met49, Met63, and Met64. On the other hand, formation of disulfide bond in DHP-A dimers precludes ET to the heme by Cys73. The number of ET pathways from six Met amino acids and Cys73 to ferric Fe makes autoreduction more amenable to a stochastic model, which can account for the probabilistic nature of these multiple pathways, rather than a model based on a defined sequence of discrete reaction pathways. In accordance with this view, we have fit the observed sigmoidal kinetics to the logistic function (Eqn. (3)).

$$\Delta c(t) = \frac{c_\infty}{1 + \tau_{1/2} e^{-k_{obs} t}} \tag{3}$$

where Φ_∞ is the asymptotic yield, $\tau_{1/2}$ is the time to half maximum, and k_{obs} is the observed autoreduction rate constant in hours^{-1}. A logistic function may also include a baseline parameter, which we have ignored because of the lack of a physical interpretation. From c_∞ for Fe^{II}–CO and the known initial concentration, c_0, one can calculate the yield of conversion, $\Phi_\infty = c_\infty / c_0$. Although the asymptotic yield Φ_∞ is obtained as a fit parameter the data only extend to the 20-h time point. Therefore, it is proper to compare the yield $\Phi_{20\ hr}$. The sigmoidal kinetics depend on internal PCET reactions by Met and Cys that lead to autoreduction and dimerization. Adding a baseline parameter would change definitions of yield, and the magnitude of $\tau_{1/2}$ and k_{obs} but trends in the data are preserved.

3. Results

The time-resolved UV–Vis spectra of the CO-driven autoreduction reaction of WT DHP-A in Fig. 2A show the transition from the ferric state with a Soret band at 406 nm and a Q band at 505 nm to the ferrous-CO state with a Soret band at 421 nm and a doublet Q band at 540 nm and 570 nm. The much sharper Soret band at 421 nm is due to the formation of six coordinated low-spin (6cLS) ferrous-CO species in contrast to the original five coordinated high-spin (5cHS) and water-ligated six coordinated high spin (6cHS) ferric state, which are known to be in equilibrium at room temperature [24,25,41]. The same transition is also observed for all the other mutants, including the H55V mutants with a 394 nm Soret band and a 507 nm Q band in the ferric state will also convert to the ferrous-CO form with Soret band at 421 nm and a doublet Q band at 539 nm and 570 nm (data not shown).

As a control experiment, the autoreduction of DHP was also conducted in a N_2 atmosphere. Autoreduction was also observed in this anaerobic control. The ferric heme was gradually reduced to the deoxy state which is indicated by the shift of both Soret band from 406 nm to 434 nm and Q bands to the characteristic broad vibronic band of the deoxy state. The autoreduction rate was circa 10-fold slower when compared to solutions under 0.1 atm CO/0.9 atm N_2. Therefore, CO is not essential for the autoreduction, but it affects the observed rate by shifting the equilibrium. Given the 50-h timeline for an experiment under N_2 atmosphere this type of anaerobic atmosphere is not practical for systematic studies. Therefore, all subsequent experiments were conducted in a 10 % CO atmosphere.

The time course of the CO-driven autoreduction reaction shown in Fig. 2 reveals that the process is not a simple second-order reaction but presents a sigmoidal kinetic behavior (Fig. 2B). Eqn. (3) characterizes the sigmoidal kinetics observed in DHP-A and mutants studied here in terms of an overall yield, Φ_∞, a time constant that defines the kinetic midpoint, $\tau_{1/2}$, and the observed rate constant, k_{obs}. Table 2 shows the trends for wild type (WT) DHPA as a function of concentration.

It was empirically observed that the autoreduction yield, $\Phi_{20\ hr}$, depends inversely on DHP-A protein concentration (Fig. 3A). The reduction of the ferric heme in the DHP-A will accelerate formation of a Fe–CO/Fe(III) heterodimer. This heterodimer traps the associated ferric heme in a conformation that hinders PCET, leading to a slower rate constant. The anti-cooperative autoreduction process is a consequence of constraints placed by dimerization on ET by Met and Cys [35]. The competition between dimerization and autoreduction is explained by the mechanism presented in Fig. 8 of the Discussion section.

Fig. 3A shows that the autoreduction rate of DHP-A is inversely proportional to the protein concentration. This observation is in contrast to the concentration-dependent reduction rate of SWMb, where the reduction rate is much slower than DHP-A and increases proportionally to SWMb concentration [34]. The fit can be improved significantly by including a baseline parameter in the fit. The difference is most notable at times less than 2 h. Fig. 3B shows the decrease in yield as a function of DHP-A concentration over the range from 15 μM to 100 μM, whereas in the case of mutated SWMb with added Cys functionality, the reduction rate was compared from 2 μM to 18 μM protein concentration [34]. The

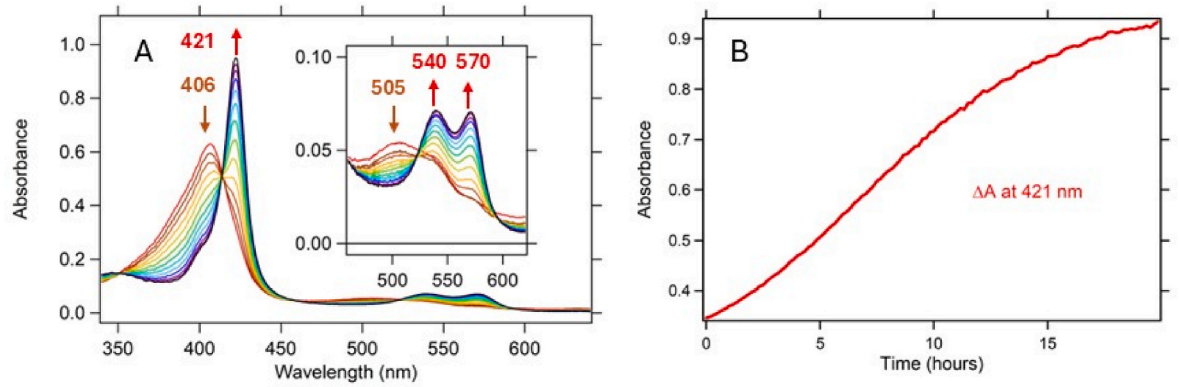

Fig. 2. The time-resolved UV–Vis spectra of CO-driven autoreduction reaction of WT DHP-A (a) and the time course of the reaction at 422 nm (b) at a concentration of 50 μM. The experiment was conducted at 37 °C in a 1 mm pathlength cuvette in 100 mM KP_i buffer at pH 7.

Table 2
Fits of the autoreduction kinetics of WT DHP-A to a logistic function as a function of concentration.

DHP-A WT	Φ_∞	$\tau_{1/2}$ (hrs)	k_{obs} (hr^{-1})
15 μ M	0.74 ± 0.05	4.0 ± 0.2	1.4 ± 0.3
25 μ M	0.72 ± 0.07	5.7 ± 0.2	1.9 ± 0.2
50 μ M	0.65 ± 0.16	8.0 ± 0.3	3.2 ± 0.3
75 μ M	0.60 ± 0.13	8.2 ± 0.7	3.4 ± 0.5
100 μ M	0.59 ± 0.12	8.0 ± 0.9	3.4 ± 0.6

inverse proportionality of rate constant and concentration extends to the low concentration regime 1.5 μM–5.0 μM [29]. While both DHP-A and SWMb have been studied for disulfide bond formation and have a similar mechanism for intermolecular association, we hypothesize that the intramolecular autoreduction rate constant of DHP-A is driven by the methionine pool. Mammalian hemoglobins and myoglobins have approximately one-third the prevalence of Met amino acids in annelids, mollusks, and bivalves that inhabit marine environments [29]. The role Met as a reductant competes with its role in protein-to-heme cross-linking. This is one possible explanation for the quantum yield of 0.65 in WT DHP-A autoreduction shown in Fig. 3 at 50 μ M.

Fig. 3C shows pH dependence of the autoreduction rate constant with an optimum pH at 7.0. Lower pH suppresses the oxidation of a cysteine residue (pK_a = 8.35) because it is more difficult to oxidize cysteine in the thiol form [42]. On the other hand, the acid-alkaline transition in DHP-A has pKa = 8.1 such that Fe^{III}–OH becomes a dominant species that slows autoreduction and decreases the yield of Fe^{II}–CO as shown in Fig. 3D [43]. Moreover, the distal histidine, H55, transition from internal to external conformation is driven by protonation with a pK_a = 6.9. In addition, CO binding affinity towards the heme decreases proportional to pH because the distal histidine His55 tends to become protonated and favor the external conformation. This conformation removes the stabilization of the distal ligand bound to the

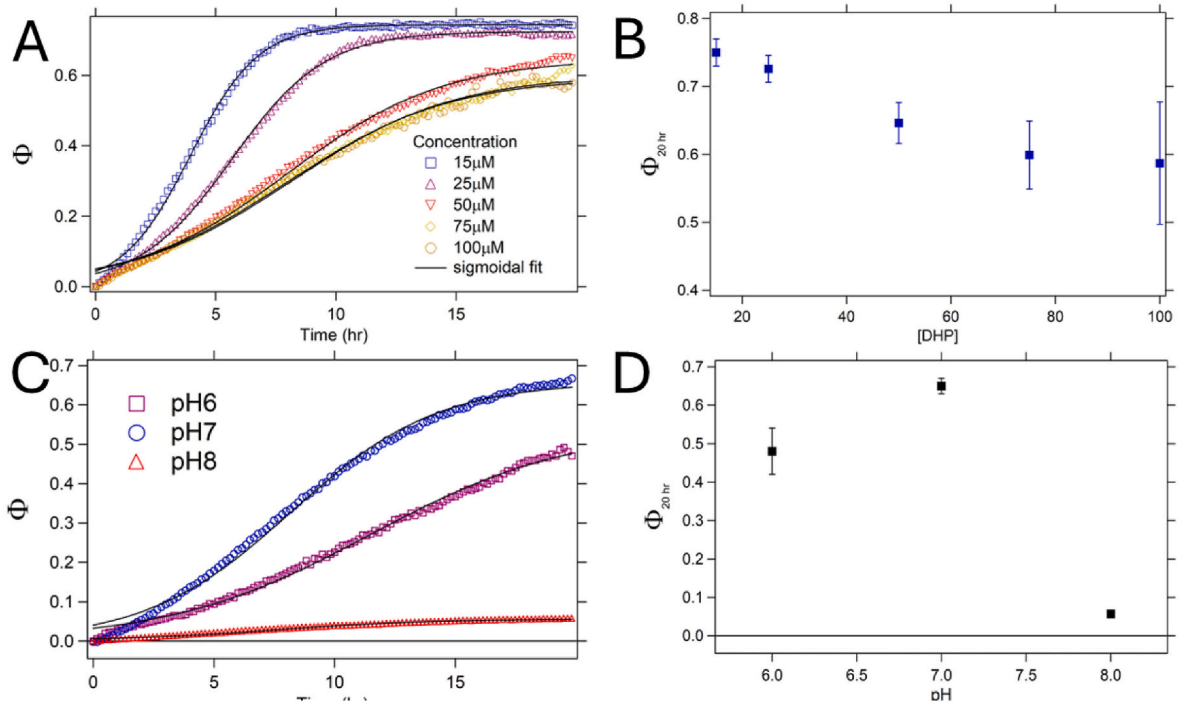

Fig. 3. (a) The DHP-A protein concentration dependence of apparent autoreduction rate at pH 7. The data are in the same order as the panel legend. (b) The yield of autoreduction at 20 h as a function of concentration at pH 7 (c) pH-dependence of the kinetics of ferrous-CO DHP at DHP-A concentration of 50 μM. The kinetic data are not in same order as the figure legend. pH 7 has the maximum autoreduction rate. (d) pH-dependence of yield of ferrous-CO DHP0A at 20 h. The experiments were conducted at 37 °C in a 1 mm pathlength cuvette in 100 mM KP_i buffer.

heme Fe [44,45]. Fits to the logistic function as a function of pH are presented in Table 3.

Fig. 4 illustrates the structural considerations in mutant selection. Cys mutations, C73S, S78C, and M49C/C73S, were selected for study to test the dimerization effect by interDHP disulfide bond formation [29]. Fig. 4A shows that the mutation S78C adds a second possible interDHP disulfide bond near the crystal dimer interface where Ser73 is located. The interdimer distances between Cys73 and Ser78 are 11.8 Å and 15.5 Å, respectively. The mutations C73S and S78C were inspired by the role of disulfide bonds in cytoglobin (Cygb) and neuroglobin (Ngb). The formation of inter- and intra-protein disulfide bonds regulates the redox states in these proteins [46]. The geometry at the opposite end of DHP is shown in Fig. 4C where M49 is featured. The M49C single mutant is not feasible because protein aggregation is observed during purification when cysteine is present at both ends of DHP. However, the double mutant C73 S/M49C moves the potential disulfide bond from position 73 to 49. The distal histidine, H55, plays a role in electron transfer, which was probed using the H55V mutation. The role of the Met amino acids in proximity to the heme vinyl group was probed by mutation to Leu using mutations M63L, M64L, and M63 L/M64L shown in Fig. 4B.

The effects of mutations on DHP-A autoreduction are shown in Table 4 and Fig. 5. The DHP-A Cys to Ser mutant (C73S) was made originally to prevent disulfide bond formation during crystallization [26]. The C73S mutant had the largest effect on the autoreduction yield, $\Phi_{20\ hr}$, which was 33 % greater than WT DHP-A. The $\tau_{1/2}$ for C73S is 23 % shorter indicating a more rapid kinetics. This result contrasts with SWMb, in which each of six Cys introduced into the sequence by site-directed mutagenesis increased the autoreduction rate by an order of magnitude [34]. Fig. 5 shows that when the Cys73 position in DHP-A was swapped from 73 to 49 in the M49C/C73S double mutant $\tau_{1/2}$ for the M49C/C73S double mutant is nearly 50 % greater. Despite the kinetic effect of mutations such as C73 S/M49C, S78C, H55V, M63L and M64L there is little effect on the autoreduction yield $\Phi_{20\ hr}$. For example, the S78C mutation exhibits essentially no change in $\Phi_{20\ hr}$ although the midpoint is reached 10 % more quickly. The only significant reduction in autoreduction yield was observed for the M63 L/M64L double mutant.

Fig. 6 shows autoreduction of DHP-A in the presence of 4-BP. The autoreduction rate constant is 2~3 times slower in the presence of 4-BP and 2,4-DBP than in the absence of internal binding molecules. 4-BP is a competitive inhibitor for DHP's peroxidase function whereas 2,4-DBP is an internal binding substrate. Both of them bind in the distal pocket of DHP with one of their bromine atoms positioned in the Xe binding site shown in Fig. 7 [41,47]. The decrease in DHP's autoreduction rate due to internal binding of 4-BP and 2,4-DBP is expected for two reasons. First, the competition between molecules like 4-BP and 2,4-DBP with diatomic gas molecule CO in the distal pocket will reduce the binding equilibrium between CO and DHP-A. Molecules like 4-BP or 2,4-DBP block the entrance of distal pocket or partially block the axial ligand binding site, which is the heme Fe. Competitive binding between fluoride ion and a range of aromatic substrates that bind internally has been used to quantify their binding constants [40]. Secondly, thin-layer spectroelectrochemistry measurement of DHP's Fe(III)/Fe(II) reduction potentials has shown that internal binding of halogenated phenols will lower DHP's positive reduction potential by about 10–25 % depending on the molecule. Substrate binding favors the heme ferric state [19].

Table 3
Fits of DHP-A autoreduction kinetics to a logistic function as a function of pH.

pH	Φ_∞	$\tau_{1/2}$ (hrs)	k_{obs} (hr^{-1})
6	0.54 ± 0.2	11.4 ± 0.3	4.2 ± 0.15
7	0.66 ± 0.15	8.2 ± 0.15	3.0 ± 0.1
8	0.06 ± 0.01	7.4 ± 0.1	3.3 ± 0.2

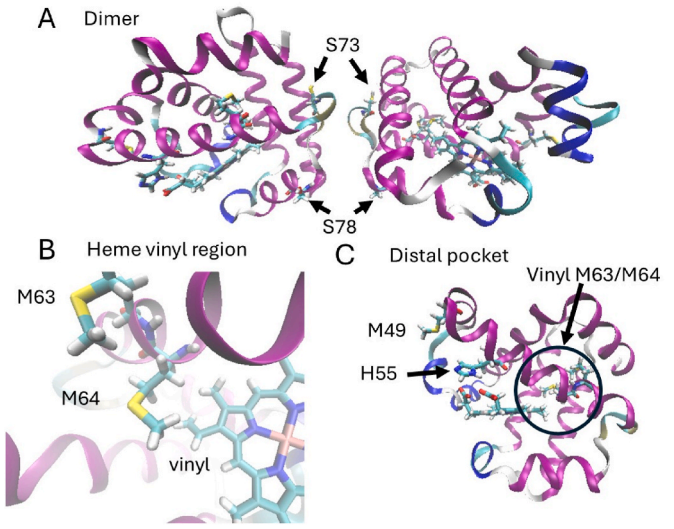

Fig. 4. Site-directed mutant structural orientation in the dimer and distal pocket. A. View of the dimer interface is shown along the C73–S78 axis. The α-helix coloring follows secondary structure. B. View of the heme vinyl region in the proximity of two methionine residues (M63/M64). C. View of the distal histidine, H55, and M49 gating the distal pocket. M49 is located on the opposite side of the protein from C73.

Table 4
Fits of the autoreduction kinetics of WT DHP-A to a logistic for seven mutants relative to wild type.

Species	Φ_∞	$\tau_{1/2}$ (hrs)	k_{obs} (hr^{-1})
WT	0.65 ± 0.10	8.0 ± 0.4	3.2 ± 0.2
M64L	0.56 ± 0.06	7.6 ± 0.2	3.1 ± 0.1
M63L	0.69 ± 0.04	7.3 ± 0.2	2.6 ± 0.1
M63 L/M64L	0.51 ± 0.07	10.5 ± 0.2	3.7 ± 0.2
C73S	0.88 ± 0.06	6.0 ± 0.1	2.5 ± 0.1
M49C/C73S	0.65 ± 0.10	9.5 ± 0.3	3.5 ± 0.1
S87C	0.65 ± 0.13	6.3 ± 0.1	2.5 ± 0.1
H55V	0.65 ± 0.12	6.1 ± 0.2	2.5 ± 0.3

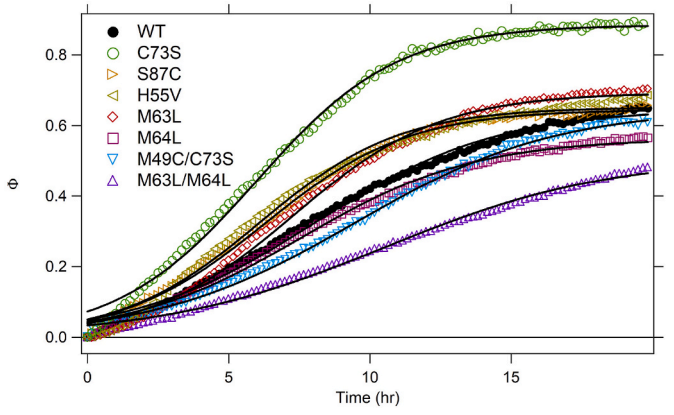

Fig. 5. The apparent kinetics and yield of the autoreduction process for DHP-A and seven mutants. The experiment was conducted at DHP-A concentration of 50 μM at 37 °C in a 1 mm pathlength cuvette in 100 mM KP_i buffer at pH 7.

4. Discussion

The autoreduction mechanism is possible only if a globin has a sufficiently high redox potential [18,19]. From a physiological standpoint autoreduction permits oxidized globins to return to the ferrous state to function as oxygen carriers without the requirement of an exogenous

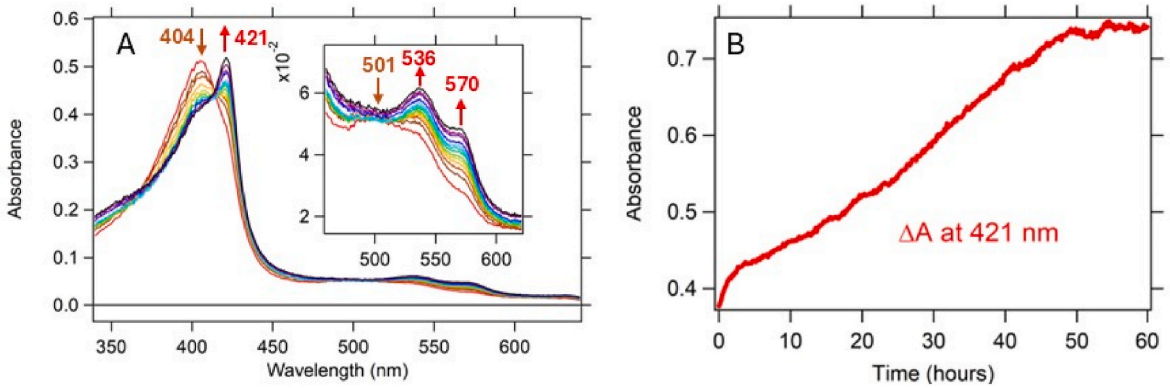

Fig. 6. The time-resolved UV–Vis spectra of CO-driven autoreduction reaction of 50 μM WT DHP-A with 1 mM 4-BP (a) time-dependent absorption spectra at 5 h delays (b) kinetics of absorbance increase at 421 nm. The experiment was conducted at 37 °C in a 1 mm pathlength cuvette in 100 mM KP_i buffer at pH 7.

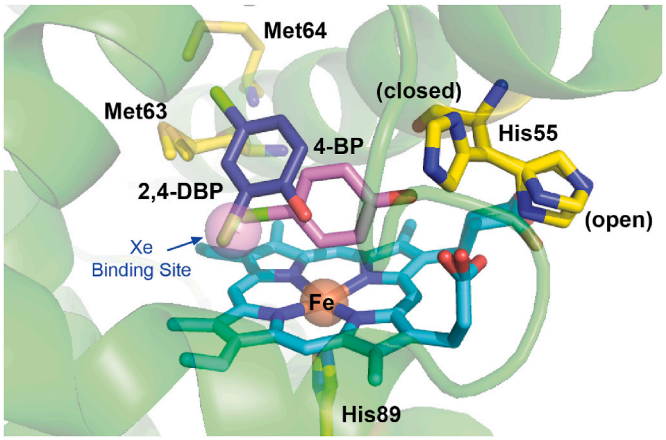

Fig. 7. The X-ray crystallography structure of internal binding of 2,4-dibromophenol (2,4-DBP) and 4-bromophenol (4-BP) in the distal pocket of DHP overlaid with structure that shown xenon binding site.

reductant. Examples of exogenous reducing proteins are flavoproteins that utilize riboflavin and ultimately NADPH [48,49] or cytochrome b_5 reductase that utilizes NADH [4,50]. Homeostasis in the red blood cells of mammals is also maintained by redox mediators such as glutathione [51,52]. There is likely a reductase system in the erythrocytes of *Amphitrite ornata*, as well. Nonetheless, DHP-A's high reduction potential ensures that it is mainly in the ferrous form despite the open distal pocket that permits entry of H_2O into the O_2-binding site of the hemoglobin which facilitates protonation of the Fe–O_2 to make superoxide anion, Fe(III)–O_2H. DHP-A admits halogenated aromatic molecules into its distal pocket where they can act as substrates or inhibitors of peroxidase function [53]. An open distal pocket would tend to accelerate autoxidation in many globins. Hence, the high reduction potential of DHP and the pool of Met amino acids both may contribute to the ability of a multifunctional catalytic hemoglobin to perform its oxygen transport function by returning to the ferrous oxidation state after one or more catalytic cycles that end with a ferric heme resting state. The reduction potentials shown in Table 5 partially explain this unique behavior of DHP-A.

The overall autoreduction rate scheme involves competition between PCET in a monomer, homodimer, or heterodimer of DHP-A. Since deprotonated Cys73 can act as an electron donor to the heme Fe in the thiolate form there is possible feedback between autoreduction and dimerization. However, it from the kinetics in Fig. 5 that dimerization Cys73 slows the autoreduction kinetics as observed in the significantly larger yield of reduced DHP-A in C73S. The mutational analysis suggests that autoreduction is primarily driven by Met amino acids, Met63 and Met64 shown in Fig. 7. Thus, autoreduction may involve Cys as an electron donor leading to disulfide bond formation and dimerization and Met as an electron donor leading to more complicated intermediates and possibly Met-heme crosslinking promoted by autoreduction. The sulfur ester of the Met sidechain acts as a reducing agent while being oxidized to sulfoxide.

Fig. 7 shows that Met63 and Met64 are poised above the heme vinyl group in an appropriate conformation for crosslinking at distances of 5.0 Å and 9.8 Å, respectively. The dynamics of Met63 place it in van der Waals' contact with a heme vinyl group [29]. The $\Phi_{20\ hr}$ yields are 5 % greater and 15 % lower for the M63L and M64L mutations, respectively. However, the autoreduction yield of the M63 L/M64L double mutant is 30 % lower than WT and the midpoint occurs at a 60 % longer time in the double mutant. As is evident in Fig. 5 the M63 L/M64L double mutant reduces autoreduction profoundly. These results suggest a special role for adjacent methionines.

The heme crosslinking by Met63 and Met64 in DHP-A can be seen as a process parallel to autoreduction [29]. Following activation of heme by H_2O_2 and formation of Tyr radical, the six Met amino acids may form a redox pool capable of reducing Tyr and crosslinking with the heme. The protein-heme crosslinking experiments both appear to involve Met and Cys despite the fact that Tyr radicals are known to form most rapidly following addition of H_2O_2 to DHP-A [30,58,59]. Therefore, crosslinking by Tyr in DHP-A does not occur under conditions where substrate is absent [29]. The pool of 6 Met in DHP-A appears to affect the fate of oxidized Tyr leading to a different outcome than vertebrate Mbs where Tyr and His can play a role in heme crosslinking. The abundance of Met amino acids is low in vertebrate Mbs and Hbs [29]. The fact that the DHP-A autoreduction rate is at least one order of magnitude more rapid than any SWMb Cys-containing mutant suggests a role for an internal reductant other than Cys73. Moreover, the DHP-A autoreduction rate is 2.5–3 times greater than HHMb or SWMb in our control experiments (data not shown). Although Tyr radicals play an important role in enzymatic turnover their oxidation requires heme activation by H_2O_2.

Fig. 8 shows a proposed mechanism for autoreduction that includes dimerization. At the outset of an autoreduction experiment the concentration of the DHP [Fe(III)] is much greater than that of DHP [FeCO] and it is mostly monomeric [35]. While DHP $[Fe(III)]_2$ is less than 1 % we can surmist that homodimers of DHP $[FeCO]_2$ are very rare because their relative abundance depends on the square of the DHP concentration. The hypothesis that homodimers of DHP [Fe(III)] have a lower concentration than DHP [Fe(III)]/DHP [FeCO] heterodimers is based on the fact that the population of the Cys radicals in DHP [FeCO] is high relative to that of DHP [Fe(III)], keeping in mind that the concentration of DHP [Fe(III)] is much higher than that of DHP [FeCO], at least in the initial phase of the reaction. The formation of Fe(III)/FeCO heterodimers outcompetes Fe(III)/Fe(III) homodimer formation because a newly formed Cys73 radical in DHP [FeCO) is more likely to encounter

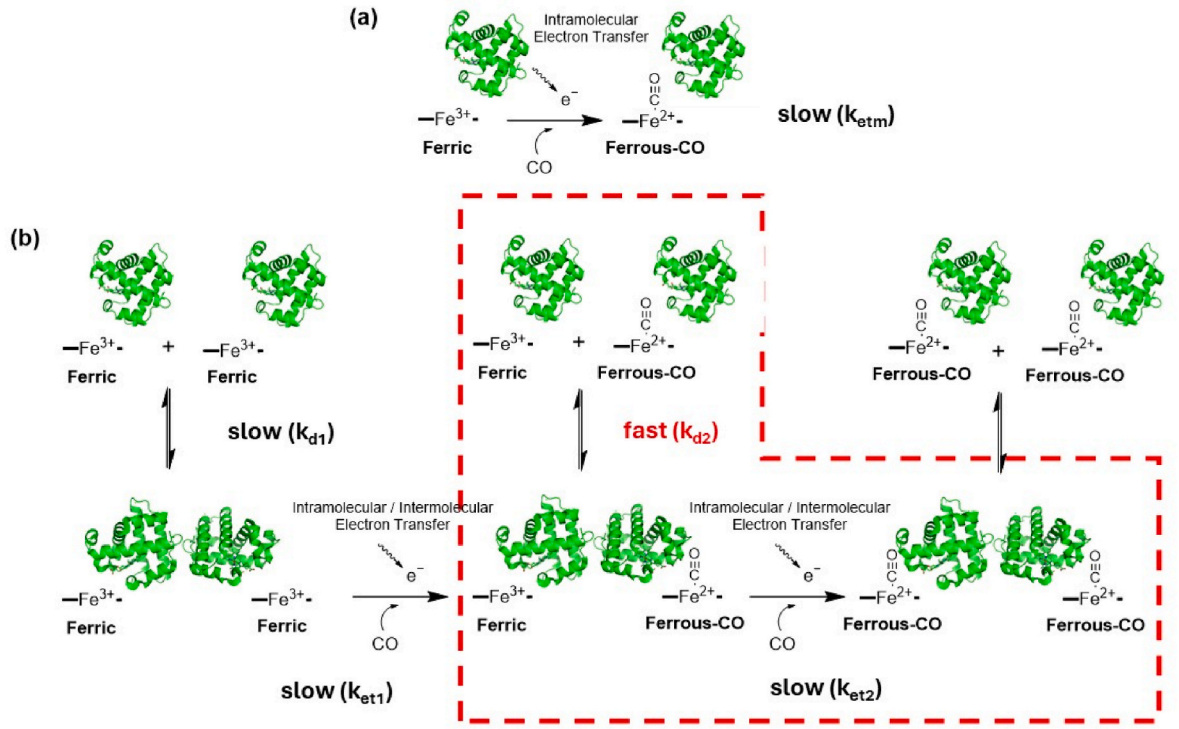

Fig. 8. (a) Monomeric autoreduction mechanism; (b) Anticooperative dimeric autoreduction mechanism.

Table 5
Reduction potentials of Various hemoglobins and myoglobins.

Heme Protein	# Cys	# Met	A.A. Length	$E^{\circ'}$ (mV)
DHP-A from *Amphitrite Ornata*	1	6	137	221 [19]
Glycera Dibranchiata Monomeric Hb	1	5	147	153[54]
Scapharca Dimeric Hb*	1	3	146	110 - 140 [55]
Human Hb beta unit	2	1	146	102[56]
Human Hb alpha unit	1	2	141	40[56]
Human Mb	1	2	154	59 [22]
Sperm Whale Mb	0	3	154	43 [57]
Horse Heart Mb	0	2	153	28 [57]

DHP [Fe(III)] than DHP [FeCO] in solution. Moreover, disulfide bond formation is catalyzed by interaction of a thiyl radical (-S •) with a reduced sulfhydryl moiety (-SH) facilitating heterodimer formation. Once a dimer is formed, the disulfide bond rules out PCET from Cys73 (k_{et1}) in that specific dimer. Therefore, the most likely electron donor becomes Met63/Met64 (k_{et2}). Dimer formation affects the dynamics of Met residues involved in intramolecular protein-heme crosslinking [29]. There are constraints on the PCET reactions in the dimer that make k_{et2} rate constant slower than the monomer k_{etm} rate constant. The complex interplay of these different pathways may explain the inverse concentration dependence of DHP-A.

Autoreduction is a complex process that includes heme dimerization, and protein-heme crosslinking controlled by as many as 12 possible protein radical intermediates, five Tyr, six Met, and one Cys. Table 4 shows the numerical values of rate parameters obtained by non-linear fitting to the logistic function. The logistic function has appropriate sigmoidal kinetics as shown in Figs. 2, 3, 5 and 6. Cys73 can act as an intramolecular electron donor, but also in intermolecular exchange leading to disulfide bond formation and dimerization. This is a k_{et1} process in Fig. 8. The S78C mutant follows the expected trend leading to a modest increase in autoreduction rate when an additional surface cysteine is introduced. However, this dependence is very weak. On the other hand, the C73S mutant which eliminates DHP-A's only cysteine results in a large increase in both autoreduction rate and yield as shown in Fig. 5. The M49C/C73S double mutant which changes the location of a surface cysteine but eliminates Met49 has a modest effect. The quantitative results for the Met mutants conform to intramolecular electron transfer, called a k_{et2} process in Fig. 8. Adjacent Met amino acids appear to play a special role, perhaps because the extra stabilization of the radical cation by delocalization [29]. If adjacent Met residues are a requirement for this crosslinking reaction the mechanism for slowing the reaction could be locking in a dimer conformation that increases the distance between Met63 and Met64.

5. Conclusion

One of the crucial aspects of a multifunctional globin is the regulation of redox state of the heme Fe atom [60]. This is a necessary property for a multifunctional protein that carries out both oxidative and oxygen transport functions. This study indicates that DHP relies on an internal pool of Met and a surface Cys to maintain or regulate a ferrous heme oxidation state. The internal Met/Cys pool of amino acids can complement external glutathione and cytochrome b_5 reductase systems that regulate the redox balance of hemoglobin in erythrocytes. Regulation of the redox state following Met oxidation can occur also by methionine sulfoxide reductase is a ubiquitous enzyme system that regulates the oxidation state of the Met pool.

A Met-heme crosslink has been observed to parallel autoreduction in its dependence on ET by both Met63 and Met64 and substrate binding. In parallel, these two Met residues are also involved in protein-heme crosslinking [29]. Met63 is in van der Waal's contact with the heme vinyl group and the more distant Met64 can help to stabilize a methionine cation radical needed for the reaction. Autoreduction occurs in the ferric state. The parallel crosslinking process occurs in compound I or II after H_2O_2 binding. On a short time scale following heme activation by H_2O_2 charge transfer by one of the five Tyr amino acids creates a compound ES species. The assignment of compound ES is an analogy with

cytochrome *c* peroxidase (CcP) where compound I is reduced by Trp191 [31,58]. Both Trp and Tyr form stable neutral radicals. When present, substrate is oxidized more rapidly than crosslink formation in H_2O_2-activated DHP-A, but the range of internal binding conformations can play an important role in function [26]. The experiments conducted here show that internal binding of substrate (2,4-DBP) or inhibitor (4-BP) in the distal pocket is also capable of regulating DHP-A's autoreduction behavior, just as their binding regulates the behavior of H_2O_2-activated DHP-A. The autoreduction rate of DHP-A may be significantly reduced by substrate binding because of a decrease in the redox potential. These observations suggest a multifaceted regulatory role for internal PCET by Met and Cys in DHP-A. It may be critical to both regulation and protection of DHP-A function that reduction by internal amino acids permits a switch from enzymatic to globin function to occur *in vivo*.

CRediT authorship contribution statement

Jing Zhao: Writing – original draft, Methodology, Formal analysis, Data curation. **Yinglu Chen:** Investigation. **Hunter Alford:** Investigation. **Stefan Franzen:** Writing – review & editing, Supervision, Resources, Project administration, Funding acquisition, Formal analysis, Conceptualization.

Declaration of competing interest

The authors collectively have no financial or other outside interests to declare. The research and authorship is entirely funded by public sources and there is no intellectual property or commercial application of the research.

Acknowledgements

This project was supported by National Science Foundation grants CHE-1609446 and CHE-2002954.

References

[1] R.E. Brantley, S.J. Smerdon, A.J. Wilkinson, J.S. Olson, The mechanism of autooxidation of myoglobin, J. Biol. Chem. 268 (1993) 6995–7010.
[2] M. Tsuruga, A. Matsuoka, A. Hachimori, Y. Sugawara, K. Shikama, The molecular mechanism of autoxidation for human oxyhemoglobin -: tilting of the distal histidine causes nonequivalent oxidation in the β chain, J. Biol. Chem. 273 (1998) 8607–8615.
[3] K. Shikama, The molecular mechanism of autoxidation for myoglobin and hemoglobin: a venerable puzzle, Chem. Rev. 98 (1998) 1357–1373.
[4] S. Bando, T. Takano, T. Yubisui, K. Shirabe, M. Takeshita, A. Nakagawa, Structure of human erythrocyte NADH-cytochrome$_5$ reductase, Acta Crystallogr., Sect. D: Struct. Biol. 60 (2004) 1929–1934.
[5] S.C. Dorman, C.F. Kenny, L. Miller, R.E. Hirsch, J.P. Harrington, Role of redox potential of hemoglobin-based oxygen carriers on methemoglobin reduction by plasma components, Art, Cells Blood Subst. and Biotech. 30 (2002) 39–51.
[6] R. Gozzelino, V. Jeney, M.P. Soares, Mechanisms of cell protection by heme oxygenase-1, Annu. Rev. Pharmacol. Toxicol. 50 (2010) 323–354.
[7] C.C. Winterbourn, Reconciling the chemistry and biology of reactive oxygen species, Nature Chem. Biol. 4 (2008) 278–286.
[8] M.L. Circu, T.Y. Aw, Reactive oxygen species, cellular redox systems, and apoptosis, Free Rad, Biol. Med. 48 (2010) 749–762.
[9] A. Hall, P.A. Karplus, L.B. Poole, Typical 2-Cys peroxiredoxins - structures, mechanisms and functions, FEBS J. 276 (2009) 2469–2477.
[10] R.L. Levine, J. Moskovitz, E.R. Stadtman, Oxidation of methionine in proteins: roles in antioxidant defense and cellular regulation, IUBMB Life 50 (2000) 301–307.
[11] G. Kim, R.L. Levine, A methionine residue promotes hyperoxidation of the catalytic cysteine of mouse methionine sulfoxide reductase A, Biochemistry 55 (2016) 3586–3593.
[12] G. Kim, S.J. Weiss, R.L. Levine, Methionine oxidation and reduction in proteins, Biochim. Biophys. Acta-General Subjects 1840 (2014) 901–905.
[13] S.X. Gu, J.W. Stevens, S.R. Lentz, Regulation of thrombosis and vascular function by protein methionine oxidation, Blood 125 (2015) 3851–3859.
[14] W.P. Vermeij, C. Backendorf, Reactive oxygen species (ROS) protection via cysteine oxidation in the epidermal cornified cell envelope, in: third ed., in: K. Turksen (Ed.), Epidermal Cells: Methods and Protocols, vol. 1195, 2014, pp. 157–169.
[15] Y. Shechter, Selective oxidation and reduction of methionine residues in peptides and proteins by oxygen exchange between sulfoxide and sulfide, J. Biol. Chem. 261 (1986) 66–70.
[16] Z. Chen, V. de Serrano, L. Betts, S. Franzen, Distal histidine conformational flexibility in dehaloperoxidase from *Amphitrite ornata*, Acta Crystallogr., Sect. D: Biol. Crystallogr. D65 (2009) 34–40.
[17] D.A. Barrios, J. D'Antonio, N.L. McCombs, J. Zhao, S. Franzen, A.C. Schmidt, L. A. Sombers, R.A. Ghiladi, Peroxygenase and oxidase activities of dehaloperoxidase-hemoglobin from *Amphitrite ornata*, J. Am. Chem. Soc. 136 (2014) 7914–7925.
[18] E.L. D'Antonio, E.F. Bowden, S. Franzen, Thin-layer spectroelectrochemistry of the Fe(III)/Fe(II) redox reaction of dehaloperoxidase-hemoglobin, J. Electroanal. Chem. 668 (2012) 37–43.
[19] E.L. D'Antonio, T.K. Chen, A.H. Turner, L. Santiago-Capeles, E.F. Bowden, Voltammetry of dehaloperoxidase on self-assembled monolayers: reversible adsorptive immobilization of a globin, Electrochem. Commun. 26 (2013) 67–70.
[20] J. Belyea, L.B. Gilvey, M.F. Davis, M. Godek, T.L. Sit, S.A. Lommel, S. Franzen, Enzyme function of the globin dehaloperoxidase from *Amphitrite ornata* is activated by substrate binding, Biochemistry 44 (2005) 15637–15644.
[21] X. Bailly, C. Chabasse, S. Hourdez, S. Dewilde, S. Martial, L. Moens, F. Zal, Globin gene family evolution and functional diversification in annelids, FEBS J. 274 (2007) 2641–2652.
[22] R. Varadarajan, T.E. Zewert, H.B. Gray, S.G. Boxer, Effects of buried ionizable amino acids on the reduction potential of recombinant myoglobin, Science (New York, N.Y.) 243 (1989) 69–72.
[23] V. de Serrano, Z.X. Chen, M.F. Davis, S. Franzen, X-ray crystal structural analysis of the binding site in the ferric and oxyferrous forms of the recombinant heme dehaloperoxidase cloned from *Amphitrite ornata*, Acta Crystallogr., Sect. D: Biol. Crystallogr. 63 (2007) 1094–1101.
[24] L. Lebioda, M.W. LaCount, E. Zhang, Y.P. Chen, K. Han, M.M. Whitton, D. E. Lincoln, S.A. Woodin, An enzymatic globin from a marine worm, Nature 401 (1999) 445.
[25] M.W. LaCount, E.L. Zhang, Y.P. Chen, K.P. Han, M.M. Whitton, D.E. Lincoln, S. A. Woodin, L. Lebioda, The crystal structure and amino acid sequence of dehaloperoxidase from *Amphitrite ornata* indicate common ancestry with globins, J. Biol. Chem. 275 (2000) 18712–18716.
[26] Mst Aktar, V. de Serrano, R.A. Ghiladi, S. Franzen, Structural comparison of substrate binding sites in dehaloperoxidase A and B, Biochemistry 63 (2024) 1761–1773.
[27] J. Zhao, M.J. Xue, D. Gudanis, H. Gracz, G.H. Findenegg, Z. Gdaniec, S. Franzen, Dynamics of dehaloperoxidase-hemoglobin A derived from NMR relaxation spectroscopy and molecular dynamics simulation, J. Inorg. Biochem. 181 (2018) 65–73.
[28] I.R. Kleckner, M.P. Foster, An introduction to NMR-based approaches for measuring protein dynamics, Biochim. Biophys. Acta-Prot. Proteom. 1814 (2011) 942–968.
[29] S. Mst Aktar, N.K.D. Madhuresh, R. Ghiladi, S. Franzen, The role of proton-coupled electron transfer from protein to heme in dehaloperoxidase, Biochim. Biophys. Acta 1873 (2024). Art. 141053.
[30] R. Dumarieh, J. D'Antonio, A. Deliz-Liang, T. Smirnova, D.A. Svistunenko, R. A. Ghiladi, Tyrosyl radicals in dehaloperoxidase: *how nature deals with Evolving an oxygen-binding Globin to biologically relevant peroxidase*, J. Biol. Chem. 288 (2013) 33470–33482.
[31] J. Feducia, R. Dumarieh, L.B.G. Gilvey, T. Smirnova, S. Franzen, R.A. Ghiladi, Characterization of dehaloperoxidase compound ES and its reactivity with trihalophenols, Biochemistry 48 (2009) 995–1005.
[32] P.M. Wood, The redox potential for dimethyl sulphoxide reduction to dimethyl sulfoxide: evaluation and biochemical implications, FEBS Lett. 124 (1981) 11–14.
[33] P.C. Jocelyn, The standard redox potential of cysteine-cystine from the thiol-disulphide exchange reaction with glutathione and lipoic acid, European J. Biochem. 2 (1967) 327–331.
[34] S. Hirota, K. Azuma, M. Fukuba, S. Kuroiwa, N. Funasaki, Heme reduction by intramolecular electron transfer in cysteine mutant myoglobin under carbon monoxide atmosphere, Biochemistry 44 (2005) 10322–10327.
[35] M.K. Thompson, S. Franzen, M.F. Davis, R.C. Oliver, J.K. Krueger, Dehaloperoxidase-hemoglobin from *Amphitrite ornata* is primarily a monomer in solution, J. Phys. Chem. B 115 (2011) 4266–4272.
[36] J. Zhao, C. Lu, S. Franzen, Distinct enzyme-substrate interactions revealed by two-dimensional kinetic comparison between dehaloperoxidase-hemoglobin and horseradish peroxidase, J. Phys. Chem. B 119 (2015) 12828–12837.
[37] A.L. Tsai, V. Berka, E. Martin, J.S. Olson, A "sliding scale rule" for selectivity among NO, CO, and O_2 by heme protein sensors, Biochemistry 51 (2012) 172–186.
[38] H.A. Ma, M.K. Thompson, J. Gaff, S. Franzen, Kinetic analysis of a naturally occurring bioremediation enzyme: dehaloperoxidase-hemoglobin from *Amphitrite ornata*, J. Phys. Chem. B 114 (2010) 13823–13829.
[39] B.A. Springer, S.G. Sligar, High level expression of sperm whale myoglobin in *Escherichia coli*, Proc. Natl. Acad. Sci. U.S.A. 84 (1987) 8961–8965.
[40] J. Zhao, J. Moretto, P. Le, S. Franzen, Measurement of internal substrate binding in dehaloperoxidase-hemoglobin by competition with the heme-fluoride binding equilibrium, J. Phys. Chem. B 119 (2015) 2827–2838.
[41] M.K. Thompson, M.F. Davis, V. de Serrano, F.P. Nicoletti, B.D. Howes, G. Smulevich, S. Franzen, Internal binding of halogenated phenols in dehaloperoxidase-hemoglobin inhibits peroxidase activity, Biophys. J. 99 (2010) 1586–1595.
[42] A.V. Peskin, C.C. Winterbourn, Kinetics of the reactions of hypochlorous acid and amino acid chloramines with thiols, methionine, and ascorbate, Free Rad. Biol. Med. 30 (2001) 572–579.

[43] K. Nienhaus, P.C. Deng, J. Belyea, S. Franzen, G.U. Nienhaus, Spectroscopic study of substrate binding to the carbonmonoxy form of dehaloperoxidase from *Amphitrite ornata*, J. Phys. Chem. B 110 (2006) 13264–13276.
[44] J. Zhao, V. de Serrano, J.J. Zhao, P. Le, S. Franzen, Structural and kinetic study of an internal substrate binding site in dehaloperoxidase-hemoglobin A from *Amphitrite ornata*, Biochemistry 52 (2013) 2427–2439.
[45] J.J. Zhao, V. de Serrano, S. Franzen, A model for the flexibility of the distal histidine in dehaloperoxidase-hemoglobin A based on X-ray crystal structures of the carbon monoxide adduct, Biochemistry 53 (2014) 2474–2482.
[46] E. Vinck, S. Van Doorslaer, S. Dewilde, L. Moens, Structural change of the heme pocket due to disulfide bridge formation is significantly larger for neuroglobin than for cytoglobin, J. Am. Chem. Soc. 126 (2004) 4516–4517.
[47] V.S. de Serrano, S. Franzen, Structural evidence for stabilization of inhibitor binding by a protein cavity in the dehaloperoxidase-hemoglobin from *Amphitrite ornata*, Biopolymers 98 (2012) 27–35.
[48] M. Wang, D.L. Roberts, R. Paschke, T.M. Shea, B.S.S. Masters, J.J.P. Kim, Three-dimensional structure of NADPH-cytochrome P450 reductase: prototype for FMN- and FAD-containing enzymes, Proc. Natl. Acad. Sci. U.S.A. 94 (1997) 8411–8416.
[49] I.F. Sevrioukova, H.Y. Li, H. Zhang, J.A. Peterson, T.L. Poulos, Structure of a cytochrome P450-redox partner electron-transfer complex, Proc. Natl. Acad. Sci. U. S.A. 96 (1999) 1863–1868.
[50] F. Elahian, Z. Sepehrizadeh, B. Moghimi, S.A. Mirzaei, Human cytochrome b_5 reductase: structure, function, and potential applications, Crit. Rev. Biotech. 34 (2014) 134–143.
[51] P.W. Buehler, A.I. Alayash, Redox biology of blood revisited: the role of red blood cells in maintaining circulatory reductive capacity, Antioxidants Redox Signal. 7 (2005) 1755–1760.
[52] J.E. Raftos, S. Whillier, P.W. Kuchel, Glutathione synthesis and turnover in the human erythrocyte *Alignment of a model Based on detailed enzyme Kinetics with experimental data*, J. Biol. Chem. 285 (2010) 23557–23567.
[53] D.J. Yun, V. de Serrano, R.A. Ghiladi, Oxidation of bisphenol A (BPA) and related compounds by the multifunctional catalytic globin dehaloperoxidase, J. Inorg. Biochem. 238 (2023) 112020.
[54] A.W. Addison, S. Burman, Ligand-dependent redox chemistry of *Glycera dibranchiata* hemoglobin, Biochim. Biophys. Acta 828 (1985) 362–368.
[55] A. Boffi, C. Bonaventura, J. Bonaventura, R. Cashon, E. Chiancone, Oxidized dimeric Scapharca inaequivalvis - CO-driven perturbation of the redox equilibrium, J. Biol. Chem. 266 (1991) 17898–17903.
[56] E.C. Abraham, J.F. Taylor, Oxidation-reduction potentials of human fetal hemoglobin and gamma chains - effects of blocking sulfhydryl groups, J. Biol. Chem. 250 (1975) 3929–3935.
[57] G. Battistuzzi, M. Bellei, L. Casella, C.A. Bortolotti, R. Roncone, E. Monzani, M. Sola, Redox reactivity of the heme Fe^{3+}/Fe^{2+} couple in native myoglobins and mutants with peroxidase-like activity, J. Biol. Inorg. Chem. 12 (2007) 951–958.
[58] M.K. Thompson, S. Franzen, R.A. Ghiladi, B.J. Reeder, D.A. Svistunenko, Compound ES of dehaloperoxidase decays via two alternative pathways depending on the conformation of the distal histidine, J. Am. Chem. Soc. 132 (2010) 17501–17510.
[59] L.M. Carey, R. Gavenko, D.A. Svistunenko, R.A. Ghiladi, How nature tunes isoenzyme activity in the multifunctional catalytic globin dehaloperoxidase from *Amphitrite ornata*, Biochim. Biophys. Acta-Prot. Proteom. 1866 (2018) 230–241.
[60] T.L. Poulos, J. Kraut, A hypothetical model of the cytochrome c peroxidase . cytochrome c electron transfer complex, J. Biol. Chem. 255 (1980) 10322–10330.